Multigrid Approximate Factorization Scheme for Two-Element Airfoil Flows

G. Volpe*
Grumman Corporate Research Center, Bethpage, New York

A fast numerical procedure for computing the inviscid transonic flow over two-element airfoil configurations is described in this paper. The doubly connected infinite domain around the two contours is conformally mapped into the annular region between two concentric circles and is covered by a stretched polar coordinate grid. Singularities introduced by the mapping are removed analytically. The continuity equation is discretized in full conservation form with appropriate upstream biasing of the difference equations in supersonic regions. The difference equations are solved by an algorithm that couples multigrid sequencing of the computational meshes with an approximate factorization scheme to sweep through the field. The scheme is fully second-order accurate in subsonic regions and partially so in supersonic zones, except locally near shock waves, and has proven stable and reliable in a wide variety of cases.

I. Introduction

THE understanding of, and the ability to predict, the flowfield over two-element airfoil configurations is presently very pertinent to aircraft design. The deployment of a leading-edge slat for maneuvering and the presence of a closely coupled canard for control are just two examples of aerodynamic configurations in which these very complicated flowfields are set up. Each element sets up large perturbation on the other, and these increase as the distance between the two airfoil elements decreases and their relative sizes increase. This problem was first attempted by Caughey.[1] However, the small perturbation approach used by Caughey is clearly inadequate unless one of the elements is substantially smaller than the other. A better description of the problem, and one that is applicable over most of the transonic flow range, is obtained with a full potential formulation. Viscous effects could be accounted for by coupling the outer inviscid flow to an inner boundary-layer flow and solving the two iteratively.

Grossman and Volpe[2] and Arlinger[3] developed relaxation algorithms to solve the full potential equation for the flow around two-element configurations. Both methods can predict the flow quite successfully, but the convergence rate that was achieved was quite slow. The convergence rate of these method is substantially slower than that achieved for the single airfoil problem, and it is so even at very low Mach numbers where the entire flow is essentially incompressible. This was caused by the topology of the numerical mesh they employed. Using a mapping technique developed by Ives,[4] the two airfoil elements are mapped into two concentric circles, with infinity becoming a single point between them. A uniform polar coordinate grid within the annular region between the two airfoil surfaces in the mapped plane does not give a good distribution of points in the physical plane, however. Thus, stretching is employed in the two coordinate directions to remedy this problem, but only a the cost of having the aspect ratio of the individual mesh cells vary by as much as two orders of magnitude through the computational plane. Another problem introduced by the mapping is the presence of a doublet representing the freestream flow in the middle of the computational plane. The difficulty of resolving the doublet numerically is apparent. All these difficulties are resolved in the present method, which employs the same mesh described in Ref. 2 and a multigrid/approximate factorization scheme to solve the full potential equation.

Multigrid techniques for solving flow problems were first described by Brandt[5] and have been highly developed for transonic flow problems by Jameson.[6] Very large improvements in convergence rates have been obtained for the single airfoil. For the two-element problems, Arlinger[7] obtained a moderate improvement in the convergence rate over that of Refs. 3 and 4 by employing the multigrid technique in the circumferential direction only, coupled with relaxation smoothing of the error on any particular mesh. Multigrid techniques have been known to prefer meshes with nearly constant aspect ratio. This could be the reason for the only modest success achieved by Arlinger. In the present method, the computational meshes are refined and coarsened in both directions. The smoothing of errors on each mesh is provided by an approximate factorization (AF) scheme similar to the one described by Jameson[6] for the single airfoil. The variability of the mesh is accounted for in establishing the factors in the AF scheme, and a careful numerical treatment of the region near infinity is done. The resulting algorithm is one order of magnitude faster than the relaxation scheme described in Ref. 3.

II. Formulation

Assuming the flow to be isentropic, it can then be described by the continuity equation

$$\frac{\partial}{\partial x}(\rho u)+\frac{\partial}{\partial y}(\rho v)=0 \tag{1}$$

where x and y are the Cartesian coordinates and ρ is the density. Assuming the flow to be also irrotational, the velocity components u and v can be expressed as gradients of a potential function ϕ, ϕ_x, and ϕ_y, respectively. ρ is related to the speed of sound a by the relation

$$\rho=(M_\infty a)^{2/(\gamma-1)} \tag{2}$$

where M_∞ is the freestream Mach number and γ the ratio of specific heats. a is evaluated from the total velocity

Presented as Paper 84-1664 at the AIAA 17th Fluid Dynamics, Plasmadynamics and Lasers Conference, Snowmass, CO, June 25-27, 1984, received July 26, 1985; revision received July 14, 1986.

*Staff Scientist.

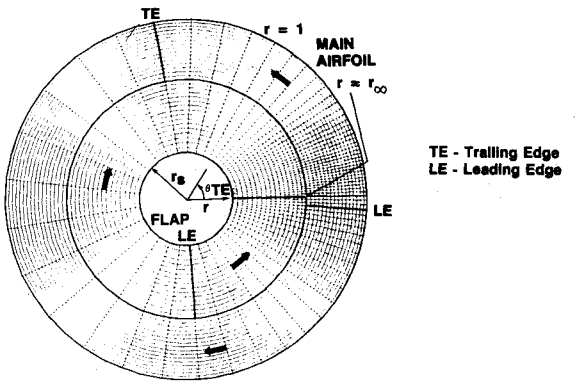

Fig. 1 Coordinate system and typical computational mesh in annular domain.

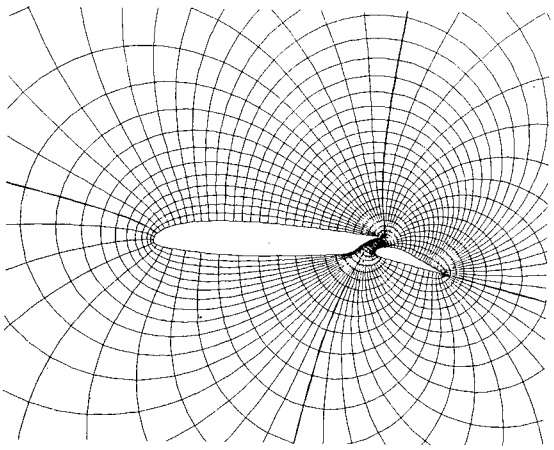

Fig. 2 Computational mesh in physical domain; 23012 airfoil with 2H flap.

$q=(u^2+v^2)^{1/2}$ by the use of Bernoulli's equation

$$a^2=a_0^2-[(\gamma-1)/2]q^2 \tag{3}$$

where a_0 is the stagnation speed of sound.

The two airfoils are mapped conformally into two concentric circles, as described by Ives.[4] The larger airfoil is mapped into a unit circle while the smaller one is mapped into a circle of radius r_s. The infinite physical domain, $z=x+iy$, becomes the annulus between the two circles in this mapped plane, $\zeta=re^{i\theta}$, with infinity becoming a single point located at a distance r_∞ from the origin. The values of r_∞ and r_s depend on the particular configuration that is mapped. For convenience, the far field is rotated in order to place the infinity point at $\theta=0$. The metric of the transformation $h=|dz/d\zeta|$ becomes singular at the infinity point. As ζ approaches $\zeta_\infty=r_\infty$, $h\to K/|\zeta-r_\infty|^2$. Here $K=K_re^{iK\theta}$ is a complex constant whose value is determined by the mapping. The metric is regularized by defining a reduced mapping function

$$H=(f/K_r)h \tag{4}$$

where $f=|\zeta-\zeta_\infty|^2$. This reduced metric H is bounded everywhere. The mapping also causes the potential function ϕ to become singular and multivalued near the infinity point. One singularity appears in the freestream part of the flow which, in the computational plane, is described by the potential function

$$\phi_D=\text{Real}\left[\frac{-Ke^{i\alpha}}{\zeta-r_\infty}\right] \tag{5}$$

where α is the angle of attack of the two-element configuration. Also, as shown in Ref. 3, the circulatory flow about the configuration is

$$\phi_C=-(\Gamma_1+\Gamma_2)\tan^{-1}[\sqrt{1-M_\infty^2}\,\tan\beta] \tag{6}$$

where Γ_1 and Γ_2 are the circulation constants about each of the two airfoil components and

$$\beta=K_\theta-\alpha+\pi+\tan^{-1}\left[\frac{r\sin\theta}{r\cos\theta-r_\infty}\right] \tag{7}$$

The flow at infinity can thus be regularized by subtracting ϕ_C and ϕ_D from the potential ϕ. ϕ_C and ϕ_D do not satisfy the boundary conditions on the circles representing the two surfaces. This generates gradients that would have to be eliminated by the numerical scheme. The gradients can, however, be eliminated analytically. A function ϕ_B that, when added to ϕ_D, resuts in a function that does satisfy the surface boundary conditions is

$$\phi_B=\sum_{n=1}^{\infty}[(A_nr^n+B_nr^{-n})\cos n\theta+(C_nr^n+D_nr^{-n})\sin n\theta] \tag{8}$$

where

$$A_n=-\frac{K_r\cos(\alpha-K_\theta)}{r_\infty^{n+1}}\left[\frac{r_s^{2n}-r_\infty^{2n}}{r_s^{2n}-1}\right] \tag{9a}$$

$$B_n=\frac{K_r\cos(\alpha-K_\theta)}{r_\infty^{n+1}}r_s^{2n}\left[\frac{1-r_\infty^{2n}}{r_s^{2n}-1}\right] \tag{9b}$$

$$C_n=\frac{K_r\sin(\alpha-K_\theta)}{r_\infty^{n+1}}\left[\frac{r_s^{2n}+r_\infty^{2n}}{r_\infty^{2n}+1}\right] \tag{9c}$$

$$D_n=\frac{K_r\sin(\alpha-K_\theta)}{r_\infty^{n+1}}r_s^{2n}\left[\frac{1+r_\infty^{2n}}{r_s^{2n}+1}\right] \tag{9d}$$

Similarly, a function ϕ_A can be added to ϕ_C such that the sum satisfies the surface boundary conditions when $M_\infty=0$. Such a function is

$$\phi_A=\sum_{n=1}^{\infty}(E_nr^n+F_nr^{-n})\sin n\theta \tag{10}$$

where

$$E_n=-\frac{(\Gamma_1+\Gamma_2)}{nr_\infty^n}\left[\frac{r_s^{2n}-r_\infty^{2n}}{r_s^{2n}-1}\right] \tag{11a}$$

$$F_n=-\frac{(\Gamma_1+\Gamma_2)}{n}\frac{r_s^{2n}}{r_\infty^n}\left[\frac{1-r_\infty^{2n}}{r_s^{2n}-1}\right] \tag{11b}$$

In practice, the infinite sums in Eqs. (8) and (10) are replaced by finite sums. Obviously, when $M_\infty=0$, the sum of ϕ_A and ϕ_B represents the solution for the flow within the annulus. Since r_∞ has a finite value, these functions are regular near the infinity point.

Thus, a reduced potential that is single-valued and bounded throughout the flowfield can be defined as

$$G=\phi-\phi_A-\phi_B-\phi_C-\phi_D-\phi_E \tag{12}$$

Here $\phi_E = \Gamma_2\theta$ is introduced in order that any closed contour about individual airfoils produce the appropriate circulation jump.

Since the mapping is conformal, the continuity equation retains the form given in Eq. (1) but with the velocity components now being the contravariant velocities $U=\phi_\theta$ and $V=r\phi_r$, and they are related to the velocity components in the radial and circumferential directions u_r and u_θ, respectively, by

$$u_\theta = fU/rK_rH, \qquad u_r = fV/rK_rH \tag{13}$$

The formulation of the problem is now basically complete. The unknown variable that described the flowfield, G, is to be found by solving the continuity equation subject to the boundary conditions on $r=r_s$ and $r=1$ that the velocity component normal to the surface, V, vanish there. Since this is a Neuman problem, the value G is kept fixed at the infinity point. The values of the circulation constants Γ_1 and Γ_2 are found by setting the tangential component of velocity U equal to zero at each of the two trailing-edge points. Since H goes to zero at these points, these Kutta conditions ensure that all velocities remain finite everywhere.

The solution for the flowfield is found by approximating the differential equation by a set of difference equations written at the node points of a mesh covering the flowfield. A mesh equally spaced in the circumferential direction in the circle plane does not give a proper concentration of points in all the regions where high gradients are expected, namely, leading and trailing edges. This is caused by the unequal distortion of the flowfield introduced by mapping infinity to one side of the annular region. The required concentration is introduced by a stretching in the circumferential direction, $X=X(\theta)$. This stretching is also used to place the two trailing-edge points exactly at grid points. A radial stretching, $Y=Y(r)$, is also introduced to locate the point of infinity midway between the two rings representing the airfoil contours. Thus, coordinate rings of radius less than r_∞ wrap around one airfoil in the physical plane, while rings with a radius larger than r_∞ wrap around the other. The r_∞ ring represents a line passing between the airfoils and going to infinity in the physical plane. A typical stretched grid, as it appears in the mapped plane and in the physical plane, is depicted in Figs. 1 and 2, respectively. As can be seen from these figures, the aspect ratio of the mesh cells varies drastically through the flowfield. This can be very troublesome in numerical schemes, and special provisions have to be made to account for the variability of the computational mesh. Another complicating factor is introduced by the doublet representing the freestream flow centered on the grid point representing infinity. In Fig. 3, the streamlines computed for a typical flow are depicted as they appear in the computational plane. Since infinity is bounded by only four mesh cells, regardless of the number of grid points in the mesh, the question of adequate resolution of the flow arises. Also, disturbances set up near the airfoil surfaces can go out to infinity through these four cells only with adverse effects on the convergence rate of a numerical scheme.

III. Numerical Procedure

Difference Approximation

In the stretched computational plane, the continuity equation becomes

$$\frac{\partial}{\partial X}(\rho U) + \frac{rY'}{X'}\frac{\partial}{\partial Y}(\rho V) = 0 \tag{14}$$

This is discretized on the stretched mesh in the computational plane in a scheme that closely follows the one proposed by Jameson for the single airfoil problem.[8] The discretization is done in full conservation form to prevent spurious mass creation by the numerical scheme as noted by Murman.[9] Following Jameson's staggered box scheme, the discretization of the equation is accomplished by performing a mass flow balance numerically through the faces of each of the cells whose corners are the centers of the mesh cells. The values of the unknown variable G and of the metric function H are stored at the nodes of mesh. Thus, at a point (i,j), the equation is written as

$$R_{ij} = S_{ij} + T_{ij} = [(\rho U)_{i+\frac{1}{2},j} - (\rho U)_{i-\frac{1}{2},j}] + \frac{rY'}{X'}\frac{\Delta X}{\Delta Y}[(\rho V)_{i,j+\frac{1}{2}} - (\rho V)_{i,j-\frac{1}{2}}] = 0 \tag{15}$$

where X' and Y' are the first derivatives of the stretching functions and ΔX and ΔY are the mesh spacings of the final computational mesh. The value of R_{ij}, the residual, represents the departure of the difference equation from the solution. It is the quantity that must be driven to zero. Since the computational mesh is orthogonal and of constant spacing, ΔX and ΔY, each mass flow cell intersects the mesh cell midway between nodes. The velocities U and V are obtained from the reduced potential. Thus,

$$U_{i+\frac{1}{2},j} = \frac{X'}{\Delta X}(G_{i+1,j} - G_{i,j}) + (\phi_{A_\theta} + \phi_{B_\theta} + \phi_{C_\theta} + \phi_{D_\theta} + \phi_{E_\theta})_{i+\frac{1}{2},j} \tag{16}$$

$$V_{i,j+\frac{1}{2}} = r\left[\frac{Y'}{\Delta Y}(G_{i,j+1} - G_{i,j}) + (\phi_{A_r} + \phi_{B_r} + \phi_{C_r} + \phi_{D_r})_{i,j+\frac{1}{2}}\right] \tag{17}$$

with similar expressions for $U_{i-\frac{1}{2},j}$ and $V_{i,j-\frac{1}{2}}$. $U_{i+\frac{1}{2},j}$ and $V_{i+\frac{1}{2},j}$ are averaged at the mesh cell center they straddle and, using an interpolated value of the metric, the physical velocity components, u_r and u_θ, the speed of sound, and the density can be computed in turn at the mesh cell centers. The values of density at the midpoints that are needed in Eq. (15) are interpolated from these cell centers quantities. A problem with this procedure is caused by the derivatives of the freestream function, ϕ_{D_θ} and ϕ_{D_r}, which appear in Eqs. (16) and (17). They, like all other analytical quantities, are stored at the node points of the mesh. They must therefore be interpolated to get the needed midpoint values. Because of the singular behavior of the freestream part, ϕ_D near the infinity point, its derivatives are also singular there. In particular as

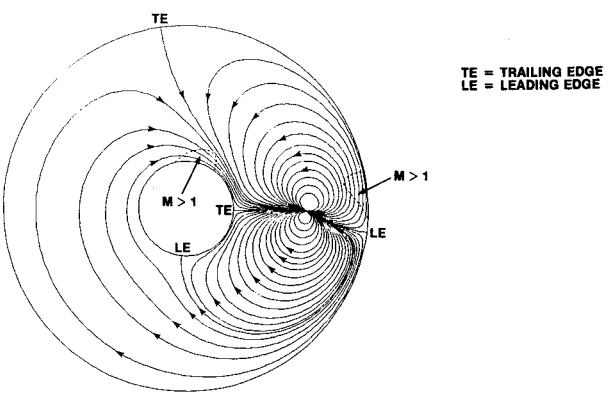

Fig. 3 Computed streamlines in annular domain; 23012 airfoil with 2H flap, $M_\infty = 0.500$, $\alpha = 2.5$ deg.

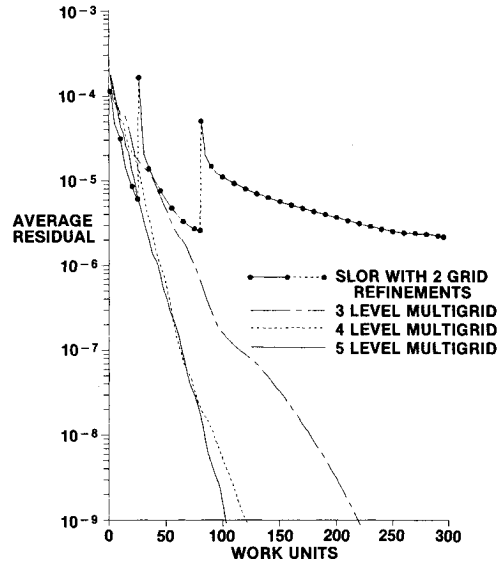

Fig. 4 Convergence history of average residual for SLOR and multigrid methods applied to AS/N1 airfoil with C6 slat, $M_\infty = 0.700$, $\alpha = 3.0$ deg.

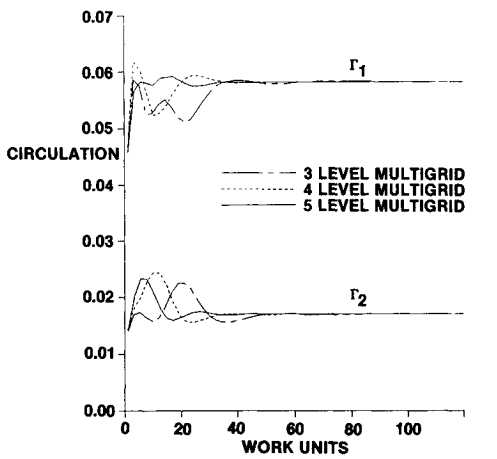

Fig. 5 Convergence history of circulation constants in multigrid method applied to AS/N1 airfoil with C6 slat, $M_\infty = 0.700$, $\alpha = 3.0$ deg.

$\theta \to 0$ along the ring going through the infinity point ($r = r_\infty$), $\phi_{D_r} \to -[K_r \cos(\alpha - K_\theta)/f]$. But as infinity is approached along the ray corresponding to $\theta = 0$, $\phi_{D_r} \to [K_r \cos(\alpha - K_\theta)/f]$. In practice, interpolating for ϕ_{D_r} at midpoints near infinity leads to incorrect values for the computational velocity V and hence to erroneous values for the physical velocity, speed of sound, and density there. The problem becomes more serious as the mesh is refined and also as the Mach number is increased. Since ϕ_{D_θ} behaves somewhat better, the solution to this problem is to interpolate for ϕ_{D_θ}, even at points where only ϕ_{D_r} is needed, and to compute ϕ_{D_r} from the identity

$$r^2\phi_{D_r}^2 + \phi_{D_\theta}^2 = (rK_r/f)^2 \tag{18}$$

This is an expensive way of finding ϕ_{D_r} at midpoints because of the square root that has to be carried out, but it is necessary. An alternative method would be to store the values of ϕ_{D_r} at midpoints also.

In supersonic regions, an upwind bias has to be introduced in the difference equation in order to preclude the appearance of solutions with nonphysical expansion shocks, which is possible with the use of the central-difference scheme expessed in Eq. (15). Following the artificial compressibility scheme introduced by Hafez et al.,[10] the density in the first bracket of Eq. (15) is replaced by

$$\hat{\rho}_{i+\frac{1}{2},j} = \rho_{i+\frac{1}{2},j} - \mu_{ij}\Delta X \rho_X \tag{19a}$$

while the term in the second bracket is replaced by

$$\tilde{\rho}_{i,j+\frac{1}{2}} = \rho_{i,j+\frac{1}{2}} - \mu_{ij}\Delta Y \rho_Y \tag{19b}$$

with

$$\mu_{ij} = \max\{0,\ \nu_1[1 - (M_c^2/M^2)]\}$$

where M is the Mach number at the local node point. μ is activated only in supersonic region; in practice, as suggested by Jameson,[6] μ is activated at a Mach number M_c slightly less than 1. The constant ν_1 should be close to unity to prevent undue smearing of shock waves. The gradients of the density appearing in Eqs. (19a) and (19b) are to be evaluated at the node point immediately upstream along the corresponding coordinate line, using the values of the density computed at the neighboring cell centers.

The dissipation added to Eq. (15) through the use of Eqs. (19a) and (19b) goes to zero with the mesh size. Thus, this scheme is only first-order accurate in the supersonic zone, whereas it is second-order in the subsonic region. Better accuracy can be obtained by taking

$$\hat{\rho}_{i+\frac{1}{2},j} = \rho_{i+\frac{1}{2},j} - \mu_{ij}\Delta X[(\rho_X)_{i+k,j} - \epsilon(\rho_X)_{i+\ell,j}] \tag{20}$$

with $k = 0$, $\ell = -1$, if $U_{i+\frac{1}{2},j} \geq 0$ and $k = 1$, $\ell = 2$, if $U_{i+\frac{1}{2},j} < 0$. A similarly biased formula would apply to $\tilde{\rho}_{i,j+\frac{1}{2}}$. If $\epsilon = 1$, the additional dissipation will then disappear as the square of the mesh width. For $\epsilon = 0$, the first-order scheme is recovered. For stability, ϵ has to be reduced to zero in the vicinity of shock waves. However, it has not been possible as yet to run the method in a fully second-order mode (except for shock regions) because the value of ϵ in the supersonic region is typically 0.5. This difference scheme for supersonic regions is equivalent to the rotated difference scheme introduced by Jameson[11] for flows that are not well aligned with a coordinate direction.

To evaluate Eq. (19) the flowfield is swept along lines of constant Y from $X = 0$ to $X = X_{\max}$. Values of U and V at midpoints and of u_r, u_θ, and ρ at mesh cell centers are gathered in the sweep. However, only after they have been computed for grid line X_i are the residuals at X_{i-2} evaluated. At this point, all the necessary quantities needed to form $\hat{\rho}$ and $\tilde{\rho}$ are known, regardless of the sign of U there.

Iteration Scheme

When discretized according to Eq. (15), the steady-state continuity equation reduces to a system of equations in which the unknowns are the values of the reduced potential G at the node points of the mesh. The system of equations is solved by setting up an artificial time-dependent equation. The matrix of the correction of the potential, $C = [C_{ij}]$, is assumed to be proportional to the matrix of difference equations obtained from Eqs. (19), $R = [R_{ij}] = [S_{ij} + T_{ij}]$, which represents the error in the current values of G. Thus, it is assumed that

$$NC = \omega R \tag{21}$$

where ω is a relaxation factor. The speed of the iteration scheme depends on how closely the operator N approximates the operator implicit in R. The inverse of N should also be easily computable to reduce the numer of operations. In the stretched computational plane, the continuity equation can be rewritten as

$$\frac{\partial}{\partial X}(\rho U) + \left(\frac{rY'}{X'}\right)\frac{\partial}{\partial Y}(\rho V) = 0$$
$$= \rho(A_1 G_{XX} + A_3 G_{YY} + \ldots) \tag{22}$$

where

$$A_1=\left(1-\frac{u_\theta^2}{a^2}\right), \qquad A_3=\left(1-\frac{u_r^2}{a^2}\right)\frac{(rY')^2}{X'} \tag{23}$$

Thus, following the schemes proposed by Ballhaus et al.,[12] Holst and Ballhaus,[13] and Jameson,[8] a reasonable choice for N in subsonic flow is

$$N=N_1N_2=(S-A_3\delta^2_{Y_j})(S-A_1\delta^2_{X_i}) \tag{24}$$

with $\omega=\omega_pS$. Here ω_p is a relaxation parameter and δ^2_X and δ^2_Y are central second-order operators. Thus, for example,

$$\delta^2_XC_{ij}=(C_{i+1,j}-2C_{ij}+C_{i-1,j}) \tag{25}$$

S should control the damping and should reflect time-like directions. Thus, it is assumed that

$$S=S_0+S_1\delta_{\bar{X}}+S_2\delta_{\bar{Y}} \tag{26}$$

where

$$S_0=p_0X', \qquad S_1=p_1rY', \qquad S_2=p_2\frac{(rY')^2}{X'} \tag{27}$$

p_0, p_1, and p_2, are constants and $\delta_{\bar{X}}$ and $\delta_{\bar{Y}}$ are one-sided first-order operators. $\delta_{\bar{X}}$ and $\delta_{\bar{Y}}$ should be oriented in the direction the flow is coming from. However, because the corrections C_{ij} are found sequentially, X and Y sweep directions must be chosen. The flowfield is broken up into four regions delimited by $r=r_\infty$ and four radial lines joining this ring with the leading edges and trailing edges of each airfoil, as shown in Fig. 1. Each of the four regions is then swept in the direction going from the respective leading edge to the trailing edge. Then,

$$\delta_{\bar{X}}C_{ij}=C_{ij}-C_{i\pm1,j} \tag{28}$$

with the sign depending on whether i is decreasing or increasing in the particular region. For stability of the scheme, $\delta_{\bar{Y}}$ must necessarily be oriented in the direction of increasing r. Hence,

$$\delta_{\bar{Y}}C_{ij}=C_{ij}-C_{i,j-1} \tag{29}$$

Nonetheless, with this scheme, the flowfield is swept in the direction of the flow in supersonic regions in practically all cases. It breaks down only when a supersonic region becomes so large that it crosses the midring and the field is being swept in opposite directions in that area. However, in such cases, the shock waves become so strong that the potential approximation itself becomes dubious. In supersonic regions, to enhance the stability of the scheme, N is modified to be

$$N=N_1N_2=(S-A_3\delta^2_{Y_j}-\mu_{Y_j}\delta^2_{Y_j}+\mu_{Y_{j-k}}\delta^2_{Y_{j-k}})$$
$$\times(S-A_1\delta^2_{X_i}-\mu_{X_i}\delta^2_{X_i}+\mu_{X_{i-\ell}}\delta^2_{X_{j-\ell}}) \tag{30}$$

where $k=\text{sign}(v)$, $\ell=\text{sign}(u)$ and

$$\mu_{X_i}=\mu_{ij}X'\left(\frac{u_\theta}{a}\right)^2, \qquad \mu_{Y_j}=\mu_{ij}\frac{(rY')^2}{X'}\left(\frac{u_r}{a}\right)^2 \tag{31}$$

The two factors in N approximate the leading terms of the steady-state continuity equation in both subsonic and supersonic flow regions. As usual with these approximate factorization (AF) schemes, the inversion of the matrix N is done in two steps. First, the intermediate variable C' is found from

$$N_1C'=\omega_pSR \tag{32}$$

by inverting N_1. In a second step, the correction C is determined from

$$N_2C=C' \tag{33}$$

The solution of Eq. (32) is obtained by sweeping through the field along lines of constant X. The inverse of N_1 is easily computed since it is a pentadiagonal matrix. For the solution of Eq. (33), the field is swept along lines of constant Y, and again N_2 is easily inverted since it is a pentadiagonal matrix with periodic end conditions.

The underlying strategy in AF schemes is to cycle through a sequence of values of S (or, as in this case, p_0, p_1, and p_2) to damp out the errors in G. These errors can be presented as sum of eigenvectors, each corresponding to an eigenvalue of Eq. (21). Each eigenvalue reflects a particular error frequency. Cycling among several values of S thus enables a numerical scheme to damp out errors of all frequencies more quickly than they would be if a constant value were used.

Multigrid Strategy

The multiple-grid method provides a faster alternative to the parameter cycling required by an AF method. A single set of values for p_0, p_1, and p_2 is used to damp out the high-frequency errors, and the multigrid strategy provides damping for the lower frequencies. This is possible because the low frequencies of one mesh become high ones on a coarser mesh. The multigrid strategy used here closely follows the one described in Ref. 6.

After sweeping through the field a number of times, the differences between the current values of the unknown variable G and the solution are reflected in the values of the residual matrix R. Defining a nonlinear operator L^Δ, where Δ is a measure of the current mesh width, such that

$$L^\Delta G=R \tag{34}$$

an improved estimate for G can be obtained by passing on a coarser mesh of width 2Δ. The current values of G, call it $\hat{G}$, are passed on to the corresponding points on the coarser mesh. The problem defined by Eq. (21) is now solved on this coarser mesh, but with a modified operator on the right-hand side. R is replaced by a modified residual defined as

$$\bar{R}=R-L^{2\Delta}\hat{G}+I_1(L^\Delta\hat{G}) \tag{35}$$

I_1 is an injection operator. This means that the residuals computed on the fine mesh are passed on to the corresponding points on the coarse mesh. $L^{2\Delta}\hat{G}$ represent the residuals computed on the coarse mesh using the values of passed down from the higher mesh. A number of sweeps of the flowfield can be done on the coarse mesh, each time correcting the potential of this mesh. The correction ΔG to the initially injected values $\hat{G}$ can then be interpolated back to the higher mesh to provide an improved estimate of G on that mesh. Thus,

$$G_{\text{NEW}}=G+I_2(\Delta G) \tag{36}$$

The interpolation operator I_2 is cubic with typically some smoothing in the circumferential direction. The process of passing on to a coarser mesh to get improved estimates of the potential G on any particular mesh can be repeated again and again. In the present method, it is repeated until there are only four cells between the two airfoil surfaces. This means that along the radial grid line going through the infinity point, there is only one point between infinity and each of the surfaces. In cycling through the meshes, only a single sweep of the flowfield is done on any particular mesh before moving on to the next one, except on the coarsest mesh, where two sweeps are done consecutively. Each mesh damps out the errors that appear to have a high frequency on that

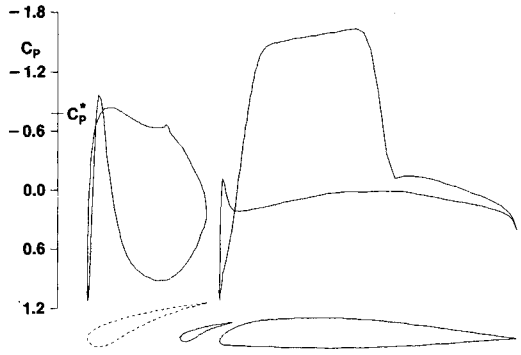

Fig. 6 Surface pressure distribution computed on AS/N1 airfoil with C6 slat, $M_\infty = 0.700$, $\alpha = 3.0$ deg.

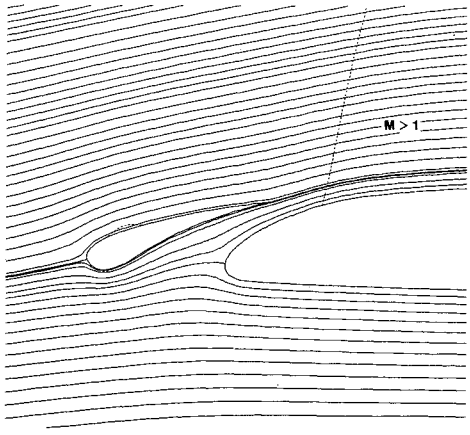

Fig. 7 Computed streamline pattern in slot region between AS/N1 airfoil and slat, $M_\infty = 0.700$, $\alpha = 3.0$ deg.

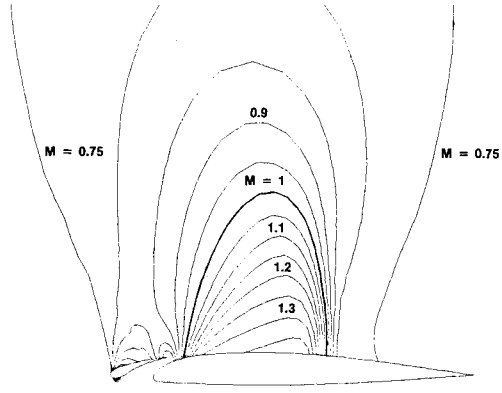

Fig. 8 Contours of constant Mach no. for AS/N1 airfoil with C6 slat, $M_\infty = 0.700$, $\alpha = 3.0$ deg.

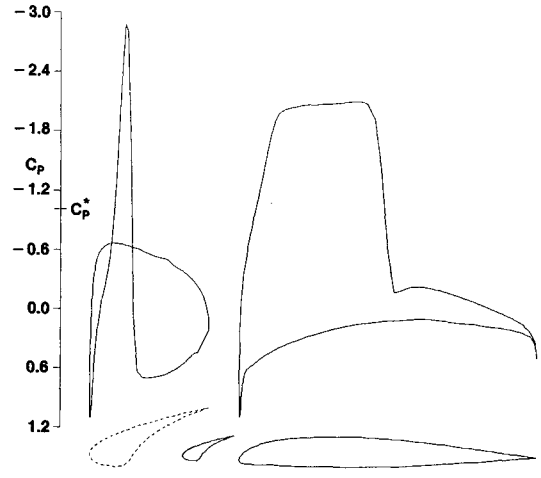

Fig. 9 Surface pressure distribution computed on AS/N1 airfoil with C5 slat, $M_\infty = 0.650$, $\alpha = 5.0$ deg.

mesh. Thus, a large range of error frequencies can be covered in one multigrid cycle, giving a rapid convergence rate. Sweeping through the field is considerably less expensive on the coarser meshes.

IV. Results and Discussions

The method has been applied to a variety of configurations and has proven to be remarkably faster than relaxation procedures for this problem and for problems such as those reported in Refs. 3 and 4. The AF multigrid method described here has displayed very good convergence rates. For some subsonic cases, convergence rates as low as 0.65 have been observed on a 128×64 point mesh with 5 multigrid meshes. The rate means that the average residual in the flowfield is reduced to 65% of its previous value by each multigrid cycle (one pass down and back up through the meshes). At transonic Mach numbers, the convergence rate is typically between 0.84 and 0.90—still greatly superior to relaxation. Despite the larger number of operations involved in carrying out an AF sweep as compared to a relaxation sweep and the additional work required to perform a multigrid cycle, the present method is still one order of magnitude faster than relaxation methods for this problem. A typical comparison of convergence histories for a typical case with a large supercritical region is presented in Fig. 4. The relaxation calculation was performed with two grid refinements, attaining a final mesh of 128 points in the circumferential direction by 64 points in the radial direction. The work unit in this case is the cost of performing one sweep of the flowfield on the final mesh. For the multigrid calculations, three cases using, respectively, three, four, and five grid levels are shown. The work unit for these cases is 1.5 times the cost of performing one sweep of the flowfield with the AF scheme on the finest (128×64) mesh. The additional factor is a rough estimate of the overhead needed to cycle through the meshes. The superiority of the present scheme is clear. Each AF sweep requires almost twice as much time as a single relaxation sweep. Thus, the actual work unit for the relaxation is smaller than the AF work unit. However, even if the relaxation curve were to be modified to reflect this factor, the superiority of the new scheme is not in doubt. It should be noted that, while the relaxation scheme gradually slows down, the convergence rate of the present method remains nearly constant. In fact, with this new method, residual levels unattainable by relaxation methods can be reached. Notice in Fig. 4 the gain in speed obtained in going from three to four multigrid meshes. The use of a fifth mesh (with 8×4 cells) gives only a marginal increase in speed. It sould be mentioned, however, that the AF coefficients, p_0, p_1, and p_2 are kept constant through the various meshes. An increase in speed could possibly be achieved if they were allowed to vary. The values of the two circulation constants, Γ_1 and Γ_2 are given as functions of the work unit in Fig. 5. The flowfield is essentially defined in 50 work units on all three meshes. With 5 mesh levels, this translates into 20 multigrid cycles.

Figure 6 depicts the pressure distribution calculated over a typical airfoil/slat configuration at a freestream Mach number of 0.700 and an angle of attack of 3 deg. The pressures for the slat are shown on an expanded horizontal scale for clarity. The true scale and the relative position of the slat relative to the main airfoil are depicted by the solid contours. As can be seen by the position of c_p^*, which

Fig. 10 Surface pressure distribution computed on Clark-Y airfoil with Maxwell slat, $M_\infty = 0.600$, $\alpha = 2.5$ deg.

Fig. 11 Surface pressure distribution computed on Clark-Y airfoil with Maxwell slat, $M_\infty = 0.600$, $\alpha = 4.0$ deg.

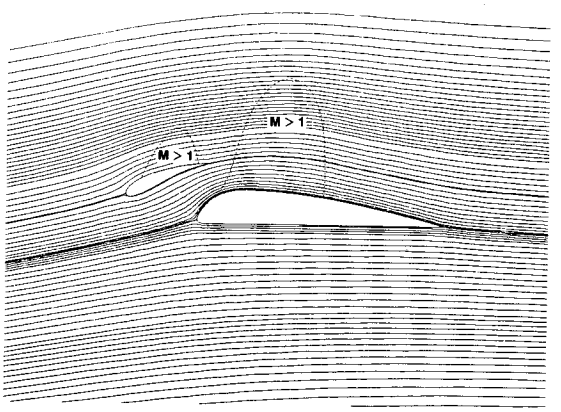

Fig. 12 Computed steamline pattern for Clark-Y airfoil with Maxwell slat, $M_\infty = 0.600$, $\alpha = 4.0$ deg.

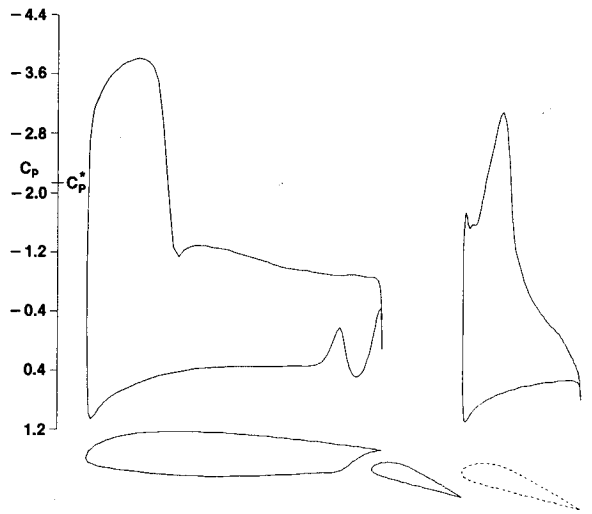

Fig. 13 Surface pressure distribution computed for 23012 airfoil with 2H flap, $M_\infty = 0.500$, $\alpha = 2.5$ deg.

denotes sonic conditions, the flow becomes supersonic over the main airfoil, and a substantial shock wave forms. The shock wave is captured usually in three to four points. The sharp expansion on the lower surface experienced by the flow near the nose of the main airfoil is due to the interference caused by the slat. The presence of the slat pulls the leading-edge stagnation streamline around the nose of the main airfoil up from the position it should have if it were isolated, thus causing the large expansion. Figure 7 shows the streamlines of the flow in the slot region. The upward pull the slat has on the stagnation streamline can be clearly seen here. The Mach number contours for this case are depicted in Fig. 8. The supersonic pocket on the main airfoil is quite large, whereas only a very small region of supersonic flow is present on the slat.

The high-lift configuration depicted in Fig. 9 consists of the same main airfoil contour shown in the previous case but with a thicker slat shape. The slat is also moved to a position slightly farther forward than in the previous example. At a Mach number of 0.650 and an angle of attack of 5 deg, a very large supersonic region is already present (as evidenced by the pressure distribution shown in Fig. 14). A considerable shock wave is present on the airfoil. The large expansion and rapid recompression calculated on the lower surface of the slat would probably cause the flow to separate in that region. In a viscous flow, this feature would therefore be mitigated considerably.

With the present method, there are no restrictions on the relative sizes of the two airfoil elements or on their relative positions. The configuration shown in Fig. 10 consists of a Clark-Y airfoil and a Maxwell-type slat. This is an old configuration developed for rotor applications. At a Mach number of 0.600 and an angle of attack of 2.5 deg, the flow over the airfoil has become highly supersonic, whereas there is only a small supercritical region on the slat, as Fig. 10 shows. As the angle of attack is increased, the supersonic region on the slat increases considerably until, at an angle of 4 deg, the shock wave on the slat reaches close to the trailing edge, as seen in Fig. 11. For this case, the flow has become so highly supercritical that the potential approximation cannot be held valid any longer. The numerical scheme held up despite the strength of the two shock waves in this flow. Figure 12 shows the computed streamline pattern and the sonic lines for this flow.

The last example is an airfoil/flap combination. This is a classical high-lift configuration. As in the previous case, it was developed for low-speed applications. Therefore, it is not surprising that supersonic flow appears even at relatively low Mach numbers. The computed pressure distribution for a freestream Mach number of 0.500 and an angle of 2.5 deg are shown in Fig. 13. The rounded leading edge on the main airfoil forces the flow to expand very quickly. A strong shock ends the supersonic region. Supercritical flow also exists on the flap. As seen on the Mach number contour chart in Fig. 14, this second region of supersonic flow begins just behind the slot region. The flow on the opposite side of the slot is, however, subsonic and actually stagnates at the sharp, pointed trailing edge. The mesh used concentrates a large number of points in the slot region, thus enabling the

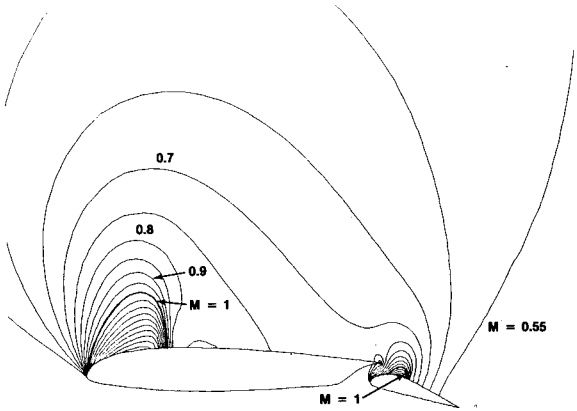

Fig. 14 Contours of constant Mach no. for 23012 airfoil with 2H flap, $M_\infty = 0.500$, $\alpha = 2.5$ deg.

numerical scheme to resolve the velocity gradients in this region very well.

All the forementioned cases were run on a 128×64 mesh, using 5 levels in the multigrid cycle. With more points clustered near the leading and trailing edges, this means that a shock wave on an airfoil contour is usually spread out approximately 5% of the chord of the airfoil. For a high Mach number case, where 30% of the mesh points are supersonic, typically 5 min are needed on an IBM 3081 to reduce the average residual of the flowfield by four orders of magnitude. At lower Mach numbers, the running time drops considerably. In addition to the faster convergence rate, the initial estimate of the flowfield gets better as the Mach number drops. The initial estimate is the exact solution in the limit of incompressible flow.

V. Conclusions

The numerical scheme presented is applicable to general two-element airfoil configurations, regardless of the relative size and position of the contours. It is partially second-order accurate in subsonic zones and locally first-order near shock waves captured without excessive smearing. The AF multigrid solver is an order of magnitude faster than relaxation schemes for this problem and, despite the fact that the mesh was highly stretched in both coordinate directions, has proved reliable in a wide a variety of cases.

Acknowledgments

The author is grateful to Professor A. Jameson of Princeton University for his helpful discussions on several aspects of this problem.

References

[1]Caughey, D., "Inviscid Analysis of Transonic, Slatted Airfoils, *Journal of Aircraft*, Vol. 13, Jan. 1976, pp. 29–35.

[2]Grossman, B. and Volpe, G., "The Viscous Transonic Flow Over Two-Element Airfoil Systems," AIAA Paper 77-688, June 1977.

[3]Arlinger, B. G., "Analysis of Two-Element High-Lift Systems in Transonic Flow," ICAS Paper 76-13, 1976.

[4]Ives, D., "A Modern Look at Conformal Mapping Including Multiply Connected Regions," *AIAA Journal*, Vol. 14, Aug. 1976, pp. 1006–1011.

[5]Brandt, A., "Multi-Level Adaptive Solution to Boundary Value Problems," *Mathematical Computation*, Vol. 31, 1977, pp. 333–390.

[6]Jameson, A., "Acceleration of Transonic Potential Flow Calculations on Arbitrary Meshes by the Multiple Grid Methods," *AIAA 4th Computational Fluid Dynamics Conference Proceedings*, Williamsburg, VA, 1979.

[7]Arlinger, B. G., "Multigrid Technique Applied to Lifting Transonic Flow Using Full Potential Equation," SAAB Rept., L-0-1 B439, 1978.

[8]Jameson, A., "A Finite Volume Method for Transonic Potential Flow Calculations," *AIAA 3rd Computational Fluid Dynamics Conference Proceedings*, Albuquerque, NM, 1977.

[9]Murman, E. M., "Analysis of Embedded Shock Waves Calculated by Relaxation Methods," *Proceedings of AIAA Conference on Computational Fluid Dynamics*, Palm Springs, CA, 1973.

[10]Hafez, M. M., Murman, E. M., and South, J. C., "Artificial Compressibility Method for Numerical Solution of Transonic Full Potential Equation," AIAA Paper 78-1148, 1978.

[11]Jameson, A., "Iterative Solution of Transonic Flow Over Airfoils and Wings Including Flows at Mach 1," *Communications on Pure and Applied Mathematics*, Vol. 27, 1974.

[12]Ballhaus, W. F., Jameson, A., and Albert, J., "Implicit Approximate-Factorization Schemes for the Efficient Solution of Steady Transonic Flow Problems," *AIAA 3rd Computational Fluid Dynamics Conference Proceedings*, Albuquerque, NM, 1977.

[13]Holst, T. L. and Ballhaus, W. F., "Fast, Conservative Schemes for the Full Potential Equation Applied to Transonic Flows," *AIAA Journal*, Vol. 17, Feb. 1979, pp. 145–152..